

Near Threshold Pulse Shape Discrimination Techniques in Scintillating CsI(Tl) Crystals

S.C. Wu^{a,b}, Q. Yue^{c,d}, W.P. Lai^{a,e}, H.B. Li^{a,b}, J. Li^{c,d}, S.T. Lin^{a,b}, Y. Liu^d,
V. Singh^a, M.Z. Wang^b, H.T. Wong^{a,*}, B. Xin^f, Z.Y. Zhou^f

^aInstitute of Physics, Academia Sinica, Taipei 115, Taiwan.

^bDepartment of Physics, National Taiwan University, Taipei 106, Taiwan.

^cDepartment of Engineering Physics, Tsing Hua University, Beijing 100084, China.

^dInstitute of High Energy Physics, Beijing 100039, China.

^eDepartment of Management Information Systems, Chung Kuo Institute of Technology, Hsin-Chu 303, Taiwan.

^fDepartment of Nuclear Physics, Institute of Atomic Energy, Beijing 102413, China.

Abstract

There are recent interests with CsI(Tl) scintillating crystals for Dark Matter experiments. The key merit is the capability to differentiate nuclear recoil (nr) signatures from the background β/γ -events due to ambient radioactivity on the basis of their different pulse shapes. One of the major experimental challenges is to perform such pulse shape analysis in the statistics-limited domain where the light output is close to the detection threshold. Using data derived from measurements with low energy γ 's and nuclear recoils due to neutron elastic scatterings, it was verified that the pulse shapes between β/γ -events are different. Several methods of pulse shape discrimination are studied, and their relative merits are compared. Full digitization of the pulse shapes is crucial to achieve good discrimination. Advanced software techniques with mean time, neural network and likelihood ratios give rise to satisfactory performance, and are superior to the conventional Double Charge method commonly applied at higher energies. Pulse shape discrimination becomes effective starting at a light yield of about 20 photo-electrons. This corresponds to a detection threshold of about 5 keV electron-equivalence energy, or 40–50 keV recoil kinetic energy, in realistic experiments.

PACS Codes: 29.40.Mc, 07.05.Kf, 84.35.+i.

Keywords: Scintillation detectors, Data analysis, Neural Networks.

*Corresponding author: Email: htwong@phys.sinica.edu.tw; Tel: +886-2-2789-6789; FAX: +886-2-2788-9828.

1 Introduction

The detection of Dark Matter and the studies of their properties [1] are of fundamental importance in particle physics and cosmology. The Weakly Interacting Massive Particles (WIMPs) are good candidates for “Cold Dark Matter”, and their experimental searches have gathered a lot of interests in recent years. The most promising avenue is to detect the nuclear recoil signatures due to elastic scatterings of WIMPs on the target isotopes. The typical energy depositions are only of the order of 10 keV, imposing big experimental challenges in terms of the detection of weak signals as well as background control at low energy close to detection threshold. A wide spectrum of experimental techniques is being pursued [1]. There is still much room for new detector concept to push the sensitivities further. It would be of great interest if the sensitivities of WIMP searches can probe the level predicted by the various Super-Symmetry models.

There are potential merits of using CsI(Tl) scintillating crystals [2] for WIMP search and other low-energy low-background experiments [3, 4]. An experiment with 200 kg of CsI(Tl) crystal scintillators to study low energy neutrino interactions at the Kuo-Sheng power reactor is being pursued [4, 5], while the adaptation of the crystal for Dark Matter searches is the focus of several R&D projects [6, 7, 8] and an on-going experiment [9].

The high-A content of the CsI enhances the sensitivities for the spin-independent interactions (which depends on the neutron number squared) between the WIMPs and the target, relative to most other candidate target isotopes. The high-Z composition allows a compact design and provides large suppression of background due to ambient radioactivity if a three dimensional fiducial volume definition can be realized. Both ^{133}Cs and ^{127}I are 100% in their respective isotopic abundance. Being close in their mass numbers, the response to nuclear recoil from the interactions with WIMPs would be similar, allowing simpler interpretations of the experimental signatures.

As a detector, the crystal has large light yield, low energy threshold and with pulse shape discrimination (PSD) characteristics for differentiating β/γ background from the nuclear recoil events [2, 5]. Scintillating NaI(Tl) crystals with the order of 100 kg target mass have been deployed for Dark Matter experiments [10], but it has been shown that CsI(Tl) provides superior PSD capabilities to NaI(Tl) [6, 9]. Unlike NaI(Tl), CsI(Tl) is only slightly hygroscopic such that it can be machined easily and does not require hermetic seal (that is, passive materials) in a large detector system. In addition, large (40 tons) electromagnetic calorimeter systems [11] have been constructed and made operational in high energy physics experiments, making this technology affordable and realistic to scale up. Considering all the associated costs, the price of CsI(Tl) is in fact less than that for NaI(Tl). In order to produce positive and definite evidence of the WIMPs, an accurate

measurement of the annual modulation (where the maximal effects are only 7%) would be necessary such that the availability of large target mass is a very desirable feature.

One of the key issues to realize a Dark Matter search experiment with CsI(Tl) crystal scintillator is the studies of the experimental signatures of nuclear recoils due to WIMP-nuclei elastic scatterings. Nuclear recoils produce high charge density (DA/dx) such that the scintillating light yield is “quenched” and the timing profile of pulse shape is different relative to the same energy deposition by minimum ionizing particles [12]. These WIMP-induced signatures are the same as the nuclear recoil events produced by elastic scattering of neutrons on nuclei, and hence can be studied in the laboratory.

2 Pulse Shape Discrimination

It has been well-studied [2, 5] that the light emission profiles of scintillating CsI(Tl) crystals exhibit different shape for γ -rays and electrons (that is, minimum ionizing particles), as compared to that for α -particles and nuclear recoils at the high energy (>100 keV) regime. Heavily ionizing events due to α -particles and nuclear recoils have *faster* decays than those from e/γ 's – opposite to the response in liquid scintillator [12]. This characteristic property makes particle identification possible with this scintillator [13].

Matured pulse shape discrimination (PSD) techniques have been devised at high energies where the photo-electrons are abundant. The experimental challenge for adapting the PSD idea to Dark Matter experiments is that one must now work in the regime where the number of photo-electrons (N_{pe}) is small such that the statistical fluctuations may wash out the differences.

In the following sub-sections, we verify that the pulse shapes of γ and nuclear recoil events with CsI(Tl) crystals are different even at the Dark Matter relevant low energy regime (<100 keV). The theme and focus of this article is to investigate and compare the various software techniques which can perform *event-by-event* PSD at this low light output domain. Detailed response characteristics of CsI(Tl) crystals at the low energy regime have already been studied in previous work [6, 7, 8, 9].

2.1 Measurements

A CsI(Tl) crystal of dimensions $5\text{ cm} \times 5\text{ cm} \times 5\text{ cm}$ and mass 560 g was used to provide data for these investigations. The light emissions were read out by a 29 mm diameter

photo-multiplier tube (PMT)[†] with standard bi-alkali photo-cathode. The conversion factor between energy deposition and light output is 4 photo-electron per keV of electron-equivalence (e.e.) energy. This was obtained by calibration measurements with an LED pulser operated at the $N_{pe} \sim 1$ intensity. The events were digitized by a 20 MHz (that is, 50 ns for one time-bin) Flash Analog-to-Digital Converter (FADC) [14] with 8-bit resolution, such that the pulse shape can be denoted by an amplitude time-sequence A_i .

The low energy γ -data were taken with a standard radioactive ^{133}Ba source, which provides several γ -lines up to 356 keV. The series of associated γ -peaks provide good energy calibration at low energy. The low energy (<30 keV) events crucial for this study are due to Compton scatterings of the higher energy γ 's such that they originate from the bulk of the crystal. These merits justify the choice of ^{133}Ba source over other low energy sources like ^{55}Fe (5.9 keV) and ^{109}Cd (22.1 keV) where the attenuation of the γ 's due to the crystal wrapping materials is severe, and the events only originate at the surface of the crystal. Nuclear recoil data, on the other hand, were taken from the neutron facility at the 13 MV Tandem accelerator at the China Institute of Atomic Energy at Beijing. The data consisted of Time-of-Flight (ToF) measurements which helped to distinguish nuclear recoil from the other background events. The results of the quenching factor measurements were already published [8]. For completeness, α -events with ^{241}Am (5.49 MeV) source were also recorded.

The nuclear recoil pulses recorded in a neutron beam environment were contaminated by an intense accidental γ -background. The average pulse shapes for both nuclear recoil and γ -background (as identified by the ToF cut) events derived from the neutron beam measurements at a nuclear recoil e.e. energy of 4.8 keV are depicted in Figure 1. The long tails indicate there is a substantial contribution from time-uncorrelated γ -background. Upon taking averages from a large sample and subtracting the γ -background, such data are sufficient to provide a good quenching factor measurement as well as the average “*background-free*” nuclear recoil pulse shapes, as depicted in Figures 2a&b.

2.2 Average Light Emission Pulse Profiles

From the FADC measurements with γ -events and the subtraction procedures for recoil events discussed in the previous section, the *average* pulse shapes for both categories are depicted in Figures 2a&b.

In Figure 2a, the spread among the average γ -pulses between 5 keV and 40 keV are denoted by dotted lines, as compared to the solid line for the recoil pulse shape at 4.8 keV

[†]CR110, Hamamatsu Photonics, China

e.e. energy (43 keV recoil energy). Similarly, the spread among recoil pulse shapes between 4 keV and 11 keV e.e. energy (about 40 keV to 110 keV recoil energy) are defined by the dotted lines in Figure 2b, whereas the solid line denotes γ -profiles at 20 keV. It can be concluded that the energy dependence of the pulse shapes *within* the recoil and γ -data samples at this low (<100 keV) energy range is small compared to the differences in the pulse shapes *between* the recoil and γ -events. These results are consistent with those from Refs. [6, 7, 9]. Event identification is in principle possible be achieved at low energy with CsI(Tl) crystals from the pulse shape information.

The pulse shapes(A) as a function of time(t) displayed in Figures 2a&b can be fitted to an analytical form

$$A = \text{Constant} * [1 - \exp(-\frac{t}{\tau_0})] * [\frac{1}{\tau_1} \exp(-\frac{t}{\tau_1}) + \frac{r}{\tau_2} \exp(-\frac{t}{\tau_2})] , \quad (1)$$

where τ_0 is the rise time, (τ_1, τ_2) denote the fall times, and r is the ratio between the slow and fast decay components. As illustrations of the typical ranges, the best-fit values for recoil events at 4.8 keV e.e. energy and γ -events at 20 keV are tabulated in Table 1. Those for undoped CsI crystal are also shown for comparison. The values of τ_0 in CsI(Tl) are dominated by the electronics shaping rise time of 250 ns for $> \mu\text{s}$ pulses [14]. The intrinsic rise times of the CsI(Tl) scintillator are expected to ~ 125 ns and ~ 20 ns for γ - and recoil-events, respectively [2]. The difference in the decay time constants between the recoil and γ -events is the basis of pulse shape discrimination.

2.3 Data Samples

The direct measurements of Figure 1 indicate that the *average* recoil pulse shape can be derived by statistical subtraction. However, at the event-by-event level, the time-profile for photo-electron emissions of the neutron beam data set is complicated by an uncontrolled and sizable background contribution. Dark Matter searches, on the other hand, are low-count-rate experiments such that nuclear recoils due to WIMP interactions will *not* be contaminated by accidentals. Therefore the neutron beam data do not provide a realistic sample for the studies of detector response and realistic signals in WIMP searches at the event-by-event level.

As remedies, the single-event nuclear recoil pulse shape was generated by simulations, where the input included the measured pulse profile at 4.8 keV e.e. energy from Figure 2a and the parametrization of Table 1. The simulated events were convolutions of (a) a total of N_{pe} single photo-electron pulses whose timing fluctuations were generated according to the average recoil pulse shape, and (b) the single photo-electron response of the PMT and readout system for each of these pulses, provided by the LED pulser measurements.

A “self-trigger” criterion was imposed to mimic the realistic situation – that is, the time-zero of the events was defined by the first instants where the pulse was above a specified threshold. As illustrations, typical events at $N_{pe} \sim 20$ from the measured γ and simulated nuclear recoil data are displayed in Figures 3a&b, respectively. Both categories of events are similar by visual inspection, demonstrating that (a) the simulation algorithms are valid, and (b) advanced pattern recognition techniques would be necessary to achieve event identification.

Applying the same algorithm on the γ -reference profile at 20 keV shown in Figure 2b, simulated γ -events were also generated. The comparisons between the distributions of the PSD figures-of-merit among the simulated and measured γ -events at $N_{pe} \sim 60$ are depicted in Figures 4a&b. The agreement is excellent, further demonstrating the ability of the pulse shape simulation algorithms in reproducing correctly the fluctuations among individual events. The figures-of-merit will be defined and discussed in details in Section 2.4.

The excellent consistencies in Figures 4a&b between simulations and data for the $N_{pe} \sim 60$ γ -events justifies the use of the simulated nuclear recoil and γ data set (denoted by D_{nr} and D_γ , respectively) for the PSD studies discussed in subsequent sections. There are better uniformity and systematic control among the different simulated data set such that the residual systematic effects will be minimized and canceled out when comparisons are made. The input parameters to the simulation procedures can be varied to study features like sensitivities and robustness.

2.4 Classical Pulse Shape Discrimination Method

2.4.1 Double Charge Method

A well-established way to achieve PSD at high light yield is the “double charge method” [15]. This involves the comparison of the “total charge” (Q_t) and the “partial charge” (Q_p), which are the total and partial integration of the pulse, respectively. This is the standard approach with Analog Digital Convertor (ADC) based data acquisition systems where the complete pulse shape information is not available. Typically, the partial charge measurement is done by delaying the PMT pulses via cabling and both the prompt and delayed signals are read out by the ABC sampled with the same gate.

Displayed in Figure 5 is the comparison of γ and α events at the MeV energy range from data with ambient radioactivity and ^{241}Am α -source, respectively. The ranges were chosen such that Q_t and Q_p involve integration over 4 μs after trigger and *after* a delay of 0.5 μs , respectively. A γ/α separation of >99% efficiency down to about 200 keV e.e. light output can be achieved. It has been shown that PSD can be achieved even in high

energy events where the FADC measurements are saturated [16]. However, as indicated in Figure 5, one would come into difficulties to perform PSD with this simple algorithm for events at light yield below 100 keV e.e. energy.

2.5 Pulse Shape Discrimination Methods at Full Digitization

With the advent and popular usage of FADCs, complete pulse shape digitization becomes realistic. Three different pattern recognition techniques were investigated, all of which rely on the full digitization of the PMT signals.

2.5.1 Mean Time Method

The measurement of the average time for individual events by the mean time (MT) method has been used for PSD studies [6]. The mean time is defined as

$$\langle t \rangle = \frac{\sum_i (A_i t_i)}{\sum_i A_i} , \quad (2)$$

where A_i is the FADC-amplitude at time-bin t_i .

The typical $\langle t \rangle$ distributions at $N_{pe} \sim 20$ for D_{nr} and D_γ are displayed in Figure 6a, at an integration of $5 \mu s$ after the time-zero set by the trigger. It can be seen that satisfactory separation can be achieved under such conditions.

2.5.2 Neural Network Methods

The neural network (NN) methods [17] are now frequently adopted for analysis in high energy physics experiments. It has been applied to event-by-event pulse shape analysis for background identification in double beta decay searches [18]. The pedestal-subtracted FADC data within $5 \mu s$ after trigger corresponds to the input nodes of the neural network. That is, the network has $N_i=100$ input nodes denoted by $X(x_i)$ with the integrated sum normalized to unity:

$$\sum_{i=1}^{N_i} x_i = 1 . \quad (3)$$

Negative values were reset to zero. In addition, the number of hidden nodes was selected to be $N_h=25$. It has been checked that the results are independent of this choice, so long as $N_h > 20$.

Adopting the Neural Network JETNET 3.0 package [17], a function $F(X)$ is defined such that

$$F(X) = G\left(\sum_{j=1}^{N_h} u_j G\left(\sum_{k=1}^{N_i} w_{jk} x_k + \theta_j\right) + \phi_0\right) \quad (4)$$

where (u_j, w_{jk}) and (θ_j, ϕ_0) are the “weight” and “offset” coefficients, respectively, to be derived from the training samples, and the function $G(y)$ is the non-linear neuron activation function

$$G(y) = \frac{1}{2} [1 + \tanh(y)] = \frac{1}{1 + e^{-2y}} \quad , \quad (5)$$

which is the functional form characterizing a 3-layer neural network consisting of the input, hidden and output layers.

A total of $N_t=4000$ events from both the D_{nr} and D_γ data sets are used as training samples, corresponding to $T(X)=1$ and 0 , respectively. The optimal coefficients are obtained by minimizing the error function

$$E = \sum_{i=1}^{N_t} [F(X) - T(X)]^2 \quad . \quad (6)$$

Once the coefficients are derived, the procedures are applied to *independent* recoil and γ data set. The $F(X)$ -values for recoil events would be larger than those for γ -events at the same light yield. The comparisons of $F(X)$ distributions for the simulated and measured γ -data at $N_{pe} \sim 60$ are shown in Figure 4a, while those for D_{nr} and D_γ at $N_{pe} \sim 20$ are displayed in Figure 6b. It can be seen that the simulations agree well with data, while there is good separation between the recoil and γ samples.

2.5.3 Likelihood Ratio Methods

Motivated by the commonly-used of likelihood ratio test [1, 19] for the goodness-of-fit, a likelihood ratio (LR) method was devised to perform the tasks of pulse shape analysis. Similar methods are successfully applied in high energy physics data analysis in comparing likelihoods and assigning probabilities among the different hypotheses for events where many output parameters are measured. The reference profiles for neutrons and γ 's from Figure 2 are required as the input. This is different from the previous two techniques where prior knowledge of the reference profiles is not necessary.

The areas of the reference pulses are normalized to unity, and the profiles are denoted by arrays $R(r_i)$ and $\Gamma(\gamma_i)$ for the nuclear recoil and γ reference shapes, respectively. Two likelihood functions, L_r and L_γ , are defined for each event:

$$L_r = \prod_{i=1}^{N_i} r_i^{x_i} \quad ; \quad L_\gamma = \prod_{i=1}^{N_i} \gamma_i^{x_i} \quad , \quad (7)$$

where $X(x_i)$ with dimension $N_i = 100$ are the measured pulse shape information for the events to be analyzed, as defined in Section 2.5.2. The likelihood functions quantify how probable the measured pulse shapes do originate from the the reference profiles. The likelihood ratio LR defined by:

$$\text{LR} = \frac{L_r}{L_r + L_\gamma} \quad , \quad (8)$$

will test which hypothesis is more likely. The LR-values for recoil events would be larger than those for γ -events at the same light yield.

The comparisons of LR between simulated and measured γ -data at $N_{pe} \sim 60$ are shown in Figure 4b. while the typical LR distributions for the D_{nr} and D_γ data set at $N_{pe} \sim 20$ are depicted in Figure 6c. Similar to the neural network methods, there are good agreement between simulations and data, while there is satisfactory separation between the recoil and γ samples.

2.6 Comparisons

The excellent agreement depicted in Figures 4a&b between measured and simulated γ -data set justifies that valid comparisons can be made between the simulated data set D_γ and D_{nr} . To quantify, two figures of merits are defined: (a) ϵ_{90} : the survival efficiencies of D_{nr} at selections which ensure that 90% of the D_γ events are suppressed; and (b) λ_{90} : the probabilities where the D_γ events would be mis-identified as recoil signals at cuts where 90% of D_{nr} would survive. Both ϵ_{90} and λ_{90} are energy dependent, and would approach 1 and 0, respectively, at the high light yield (large N_{pe}) limits.

The variations of ϵ_{90} and λ_{90} as a function of N_{pe} for the three different methods (MT, NN, LR) are depicted in Figures 7a&b, respectively. The photo-electron number N_{pe} was adopted as the unit to characterize the light yield. In this way, the results can be directly applicable to other configurations using CsI(Tl) as the detector medium. Dotted lines in Figures 7a&b corresponds to the survival probabilities of D_γ and D_{nr} , respectively. The results indicate that the generic features that all the three methods: (a) can achieve PSD with satisfactory efficiencies ($>50\%$ γ -background rejection) at $N_{pe} > 20$; (b) can identify $>90\%$ of the D_γ background while keeping the efficiencies for D_{nr} to be $>90\%$ at $N_{pe} > 80$; and (c) give similar performance at the large light yield limit ($N_{pe} = 120$), which approaches the expected values of 1 and 0 for ϵ_{90} and λ_{90} , respectively. Comparing the relative merits among the three algorithms, the NN technique gives better performance in the low energy range. The relative merits between the LR and MT methods are similar at low statistics ($N_{pe} < 20$), while LR tends to perform better at the intermediate range ($40 < N_{pe} < 80$). Accordingly, the neural network method would be the preferred

technique in pulse shape analysis at regime where the statistics is marginal.

Tests have been performed on simulated events with different single photo-electron response functions. Results consistent with the performance parameters shown in Figures 7a&b were obtained. This shows that the results are robust and insensitive to the details of the simulation algorithms so long as the same reference profiles in Figures 2a&b are used for the photo-electron timing distributions. This indicates that the results would also be valid in measurements of CsI(Tl) crystals where the PMT response and electronics settings (such as shaping times) would be different.

3 Summary and Conclusions

This article reports the measurement of light emission pulse profiles for nuclear recoil and γ -events in CsI(Tl) crystal scintillator at the energy range relevant for Dark Matter searches (< 100 keV). The energy dependence of the profiles within the recoil and γ -samples is small compared to the differences between them. Event identification is feasible for CsI(Tl) based on pulse shape discrimination.

Various software techniques to achieve pulse shape discrimination in this “near threshold” regime were studied. The performance of the three methods based on complete pulse shape information (mean time, neural network and likelihood ratio) is superior to the matured and conventional double charge method well-demonstrated when photo-electrons are abundant. Full digitization is crucial for achieving PSD at the marginal statistics domain. Among the three methods studied, the neural network technique provides the best performance in regime where the statistics is marginal, while the other two methods are still satisfactory. The algorithms are robust and insensitive to the measurement parameters like PMT response or electronic shaping times.

The results from this study are relevant to the potential capabilities and practical design of Dark Matter experiments based on the CsI(Tl) crystal. Satisfactory (bigger than 50%) separation between γ and nuclear recoil events can be achieved when the photo-electron statistics is larger than 20, which corresponds to an electron-equivalence energy threshold of about 5 keV, or 40–50 keV recoil kinetic energy, in the adopted detector configuration of 0.56 kg target mass. In realistic Dark Matter experiments, the modular mass for the CsI(Tl) target will have to be bigger, such as at the range of several kg. To maintain or even improve on such threshold, the light transmission within the crystal and the optical coupling between the crystal surface and the PMT photo-cathode will have to be optimized. Larger PMT readout surfaces as well as green-extended photo-cathodes to match the spectral emissions of CsI(Tl) can be used. Photon detectors with higher

quantum efficiencies, such as avalanche photo-diodes, can also be considered, though these devices tend to be limited in the active surface area.

Although this article focuses on data with CsI(Tl) crystal scintillators for Dark Matter searches, the software techniques are readily applicable to other detector systems for other experiments where pulse shape analysis of individual events can provide useful information. A universal reference pulse profile was adopted in the present studies, one for recoil and one for γ events, for the entire energy range of interest. This is justified in view of Figures 2a&b such that the results in Figures 7a&b are valid for CsI(Tl) crystals. In other detector systems where there may be a stronger energy dependence of the pulse shapes (as in the case for γ -events with NaI(Tl) crystals [6]), the PSD procedures can be further refined by having a different reference profile for every energy bin. The profiles can be derived from measurements with neutron beam and radioactive γ -sources like in this work. In addition, the conclusions on the relative merits among the different PSD methods are expected to be applicable to other pulse shape analysis problems where the statistics are marginal.

Besides differentiating β/γ -background from nuclear recoil events, these studies may help to lower the detection threshold by suppressing electronic noise and microphonism where the pulse shapes are in general different from those of the signals. Experiments which need *both* low threshold and background may potentially benefit from these techniques. Alongside with Dark Matter experiments, such requirements are critical in the search of neutrino magnetic moments [4] and in the measurement of the coherent scatterings of the neutrinos on the nuclei [20].

The authors would like to thank Drs. S.K. Kim and Y.D. Kim for fruitful discussions and helpful comments, and are grateful to the technical staff from CIAE and IHEP for assistance in the neutron beam data taking. This work was supported by contracts CosPa 89-N-FA01-1-4-2 from the Ministry of Education, Taiwan, NSC 89-2112-M-001-056, NSC 90-2112-M-001-037 and NSC 91-2112-M-001-036 from the National Science Council, Taiwan, and NSF19975050 from the National Science Foundation, China.

References

- [1] See the respective sections in *Review of Particle Physics*, Particle Data Group, Phys. Rev. **D 66** (2002), for details and references.
- [2] H. Grassmann, E. Lorentz and H.G. Moser, Nucl. Instrum. Methods **228**, 323 (1985); P. Schotanus, R. Kamermans, and P. Dorenbos, IEEE Trans. Nucl. Sci. **37**, 177 (1990).
- [3] H.T. Wong et al., Astropart. Phys. **14**, 141 (2000).
- [4] H.T. Wong and J. Li, Mod. Phys. Lett. **A 15**, 2011 (2000);
H.B. Li et al., TEXONO Coll., Nucl. Instrum. Methods **A 459**, 93 (2001);
H.B. Li et al., TEXONO Coll., Phys. Rev. Lett. **90**, 131802 (2003).
- [5] Y. Liu et al., TEXONO Coll., Nucl. Instrum. Methods **A 482**, 125 (2002).
- [6] G. Gerbier et al., Astropart. Phys. **11**, 287 (1999);
S. Pecourt et al., Astropart. Phys. **11**, 457 (1999).
- [7] V.A. Kudryavtsev et al., Nucl. Instrum. Methods **A 456**, 272 (2001).
- [8] M.Z. Wang et al., Phys. Lett. **B 536**, 203 (2002).
- [9] H. Park et al., Nucl. Instrum. Methods **A 491**, 460 (2002);
T.Y. Kim et al., Nucl. Instrum. Methods **A 500**, 337 (2003).
- [10] R. Bernabei et al., Phys. Lett.**B 480**, 23 (2000), and references therein.
- [11] Y. Kubota et al., CLEO Coll., Nucl. Instrum. Methods **A 320**, 66 (1992);
E. Aker et al., Crystal Barrel Coll., Nucl. Instrum. Methods **A 321**, 69 (1992);
K. Miyabayashi, Belle Coll., Nucl. Instrum. Methods **A 494**, 298 (2002);
B. Lewandowski, BaBar Coll., Nucl. Instrum. Methods **A 494**, 303 (2002).
- [12] See, for example, J.B. Birks, *Theory and Practice of Scintillation Counting*, Pergamon (1964).
- [13] J. Alarja et al., Nucl. Instrum. Methods **A 242**, 352 (1982);
F. Benrachi et al., Nucl. Instrum. Methods **A 281**, 137 (1989).
- [14] W.P. Lai et al., TEXONO Coll., Nucl. Instrum. Methods **A 465**, 550 (2002).
- [15] C.L. Morris et. al., Nucl. Instrum. Methods **137**, 397 (1976);
M.S. Zucker and N. Tsoupas, Nucl. Instrum. Methods **A 299**, 281 (1990).

- [16] Q. Yue et al., Nucl. Instrum. Methods **A 511**, 408 (2003).
- [17] See, for example,
C. Peterson, T. Rognvaldsson and L. Lonnblad, Comput. Phys. Comm. **81**, 185 (1994);
C.M. Bishop, *Neural Networks for Pattern Recognition*, Clarendon Press, Oxford (1995).
- [18] B. Majorovitis and H.V. Klapdor-Kleingrothaus, Eur. Phys. J. **A 6**, 463 (1999).
- [19] S. Baker and R.D. Cousins, Nucl. Instrum. Methods **221**, 125 (1984), and references therein.
- [20] H.B. Li and H.T. Wong, J. Phys. **G 28**, 1453 (2002).

Crystal	Event Type	Rise Time [τ_0 (ns)]	Decay Time Constant		Ratio (r)
			Fast Comp. [τ_1 (μ s)]	Slow Comp. [τ_2 (μ s)]	
CsI(Tl)	nuclear recoils	280 ± 50	0.54 ± 0.1	2.0 ± 0.2	0.29 ± 0.02
CsI(Tl)	γ	296 ± 50	1.3 ± 0.1	4.50 ± 0.4	0.58 ± 0.06
CsI(pure)	γ	~ 0.55	0.19 ± 0.02	—	—

Table 1: Fitted rise and decay time constants as well as the ratio between slow and fast decay components for recoil and γ events measured by CsI(Tl) and undoped CsI.

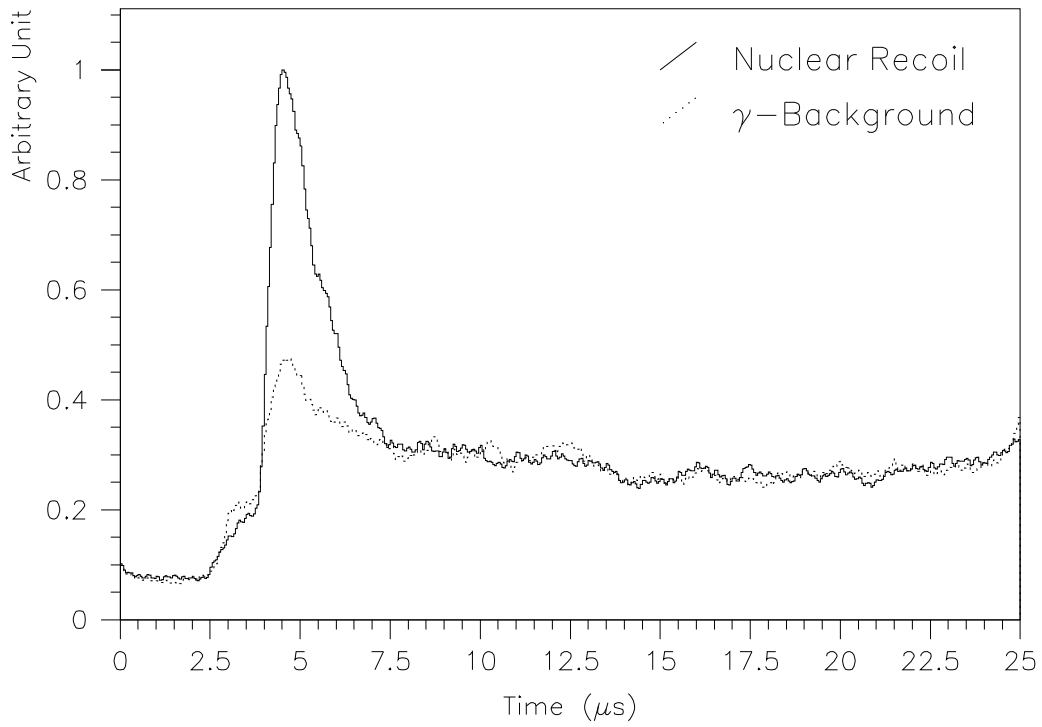


Figure 1: The average pulse shapes at 4.8 keV electron-equivalence energy for the nuclear recoil and γ -background events directly from the neutron beam measurements.

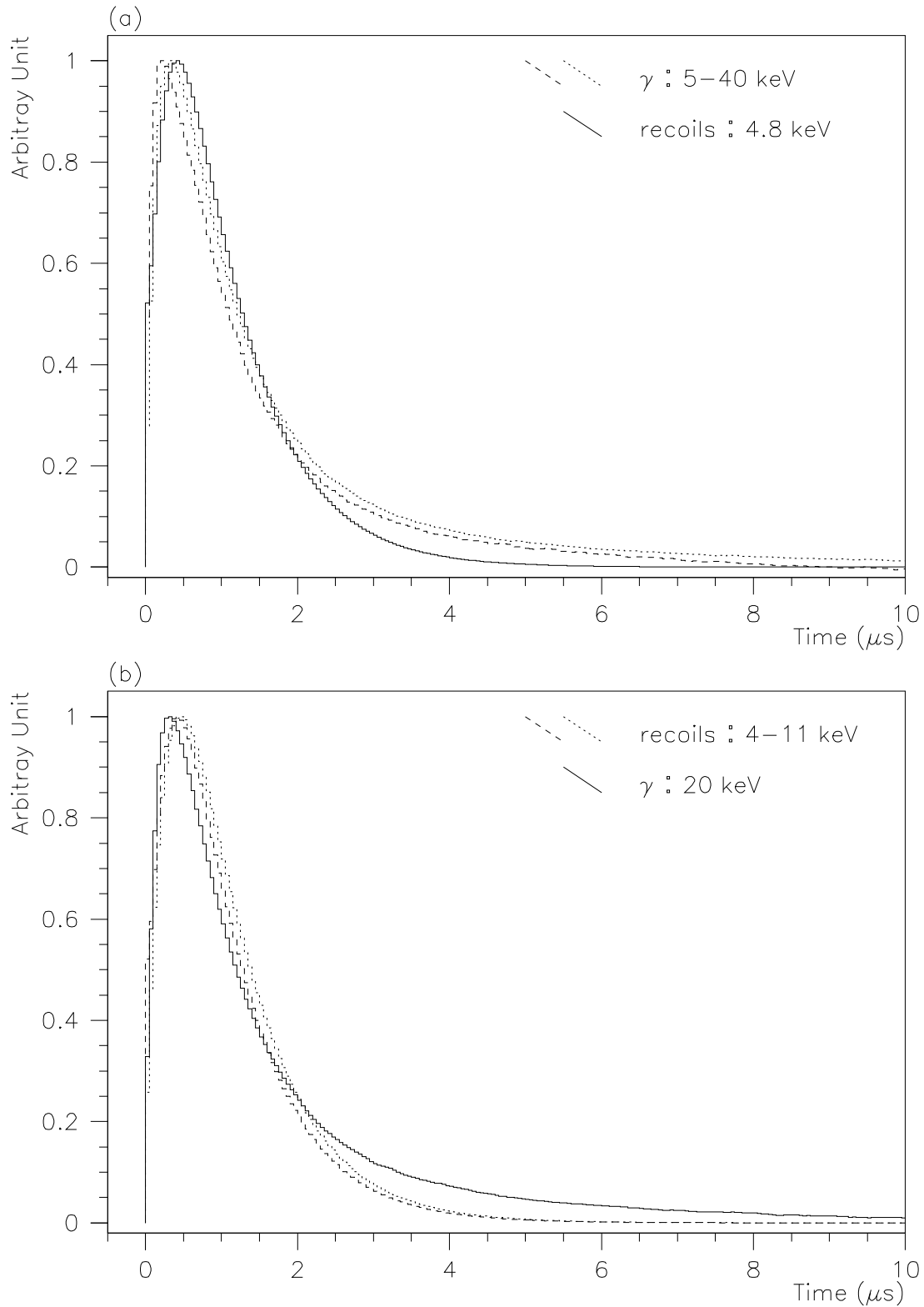


Figure 2: Comparison of average pulse shapes between γ - and nuclear recoil events: (a) recoil pulse at 4.8 keV electron-equivalence energy as compared to γ -events from 5 keV to 40 keV; (b) γ -pulse at 20 keV as compared to recoil profiles from 4 keV to 11 keV electron-equivalence energy.

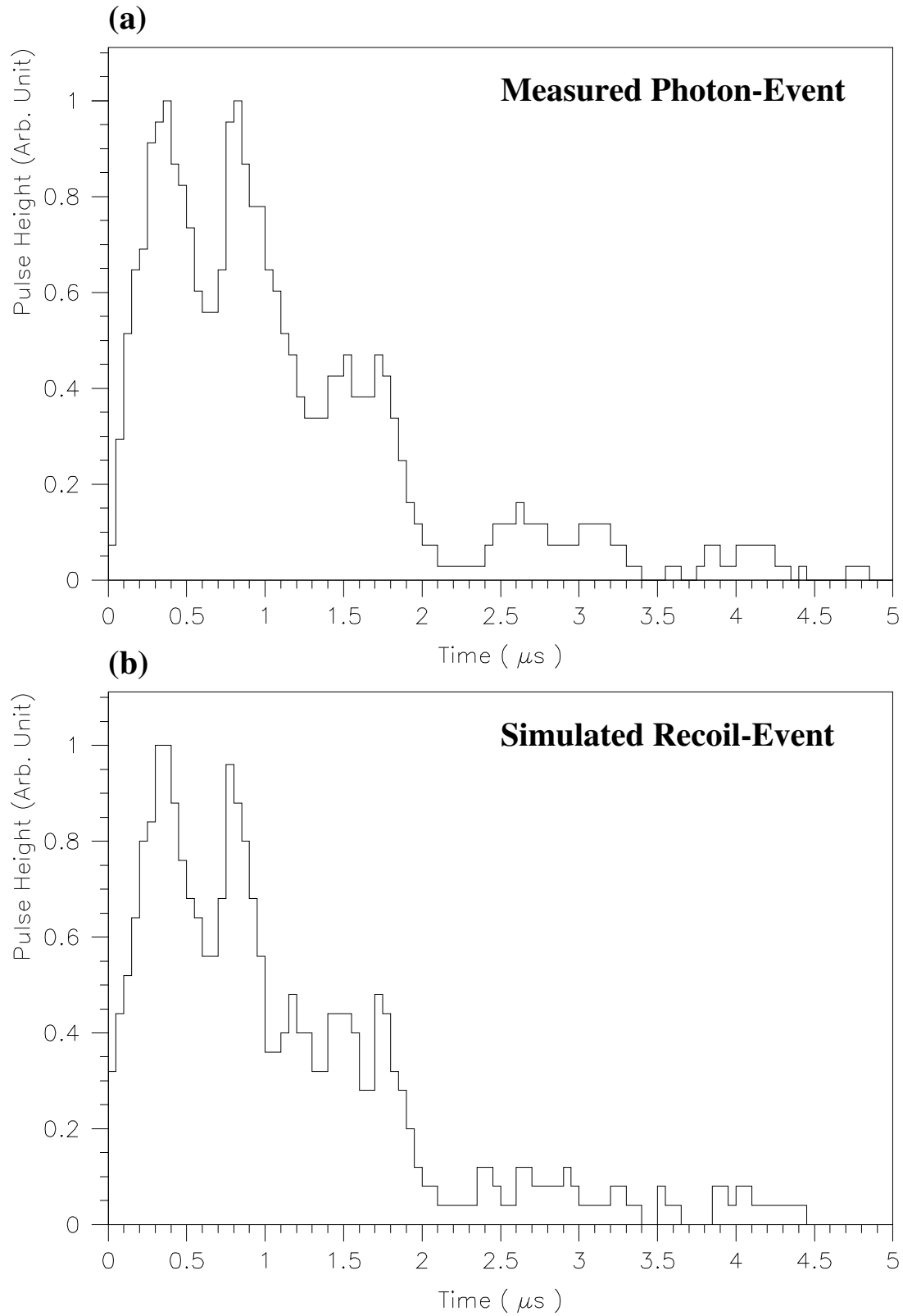
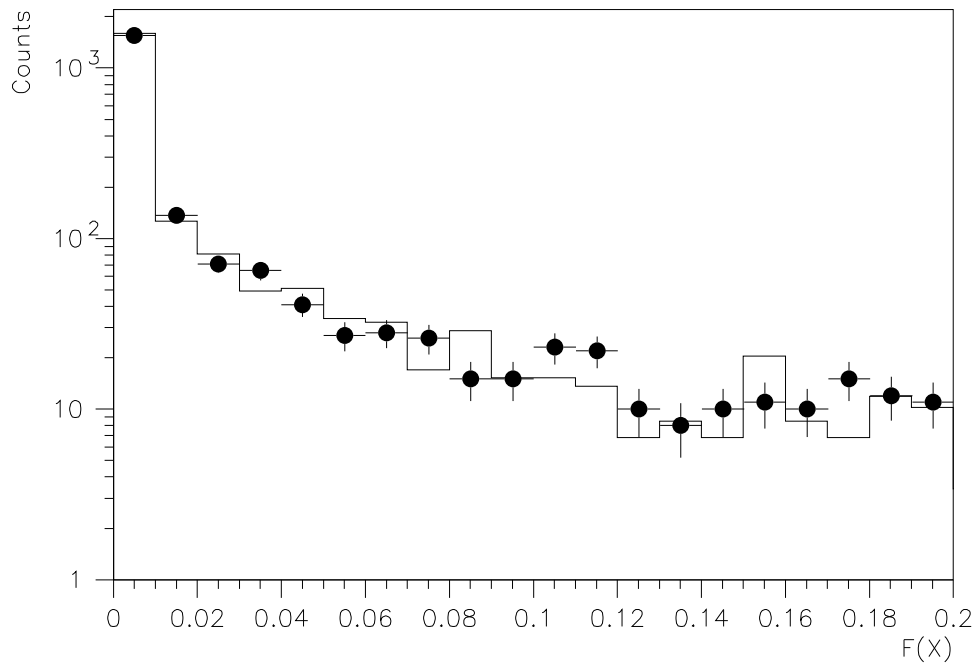


Figure 3: Typical single (a) measured γ - and (b) simulated nuclear recoil events at $N_{pe} \sim 20$.

(a)



(b)

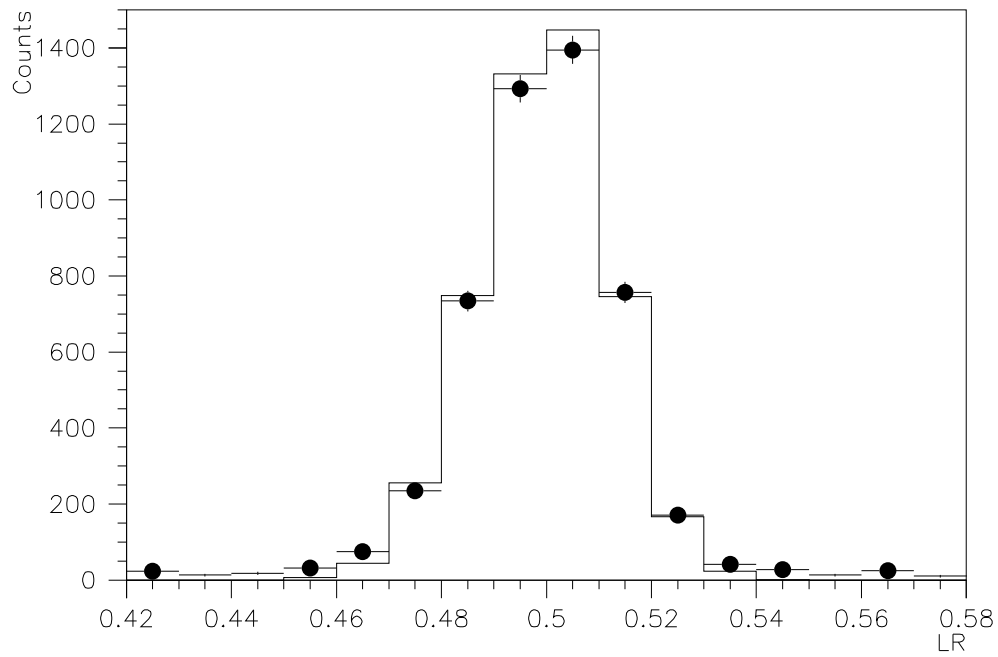


Figure 4: Comparison of the distributions of (a) $F(X)$ and (b) LR parameters between measured and simulated data denoted by solid circles and histograms, respectively.

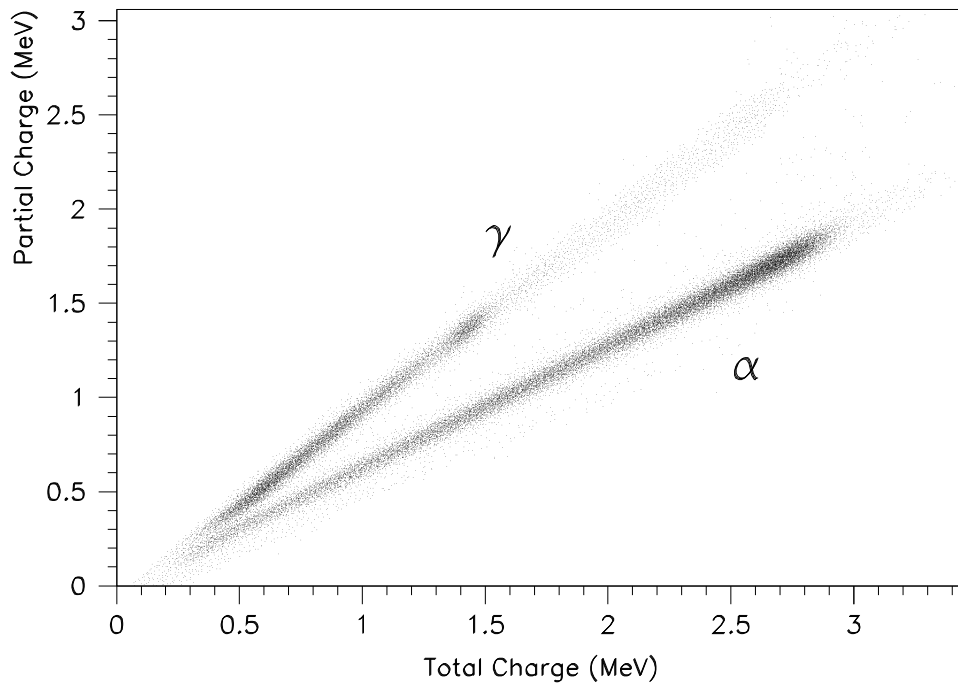
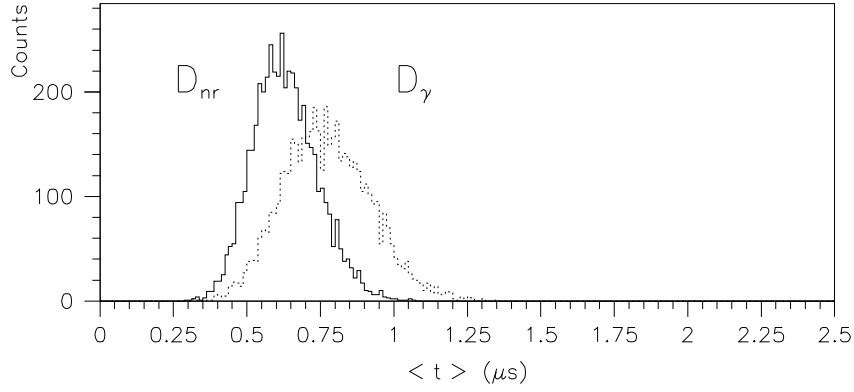
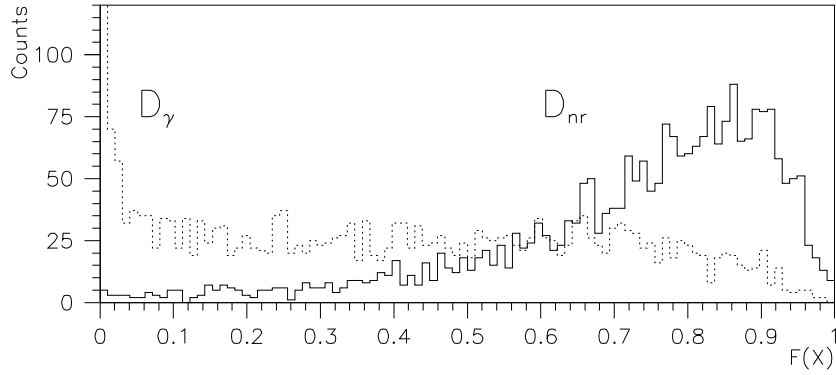


Figure 5: The partial charge versus total charge at the high (MeV) energy range in a CsI(Tl) crystal, showing excellent ($>99\%$) pulse shape discrimination capabilities to differentiate events due to α 's and γ 's. The α -events are from an ^{241}Am source (kinetic energy 5.49 MeV) placed on the surface of the crystal, while the γ -events are due to ambient radioactivity.

(a)



(b)



(c)

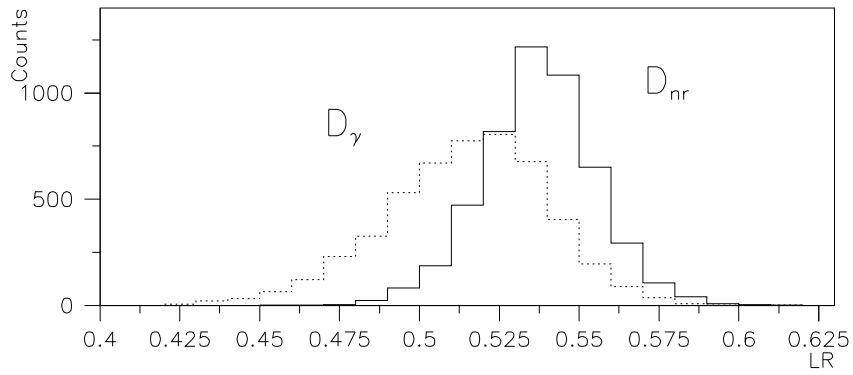
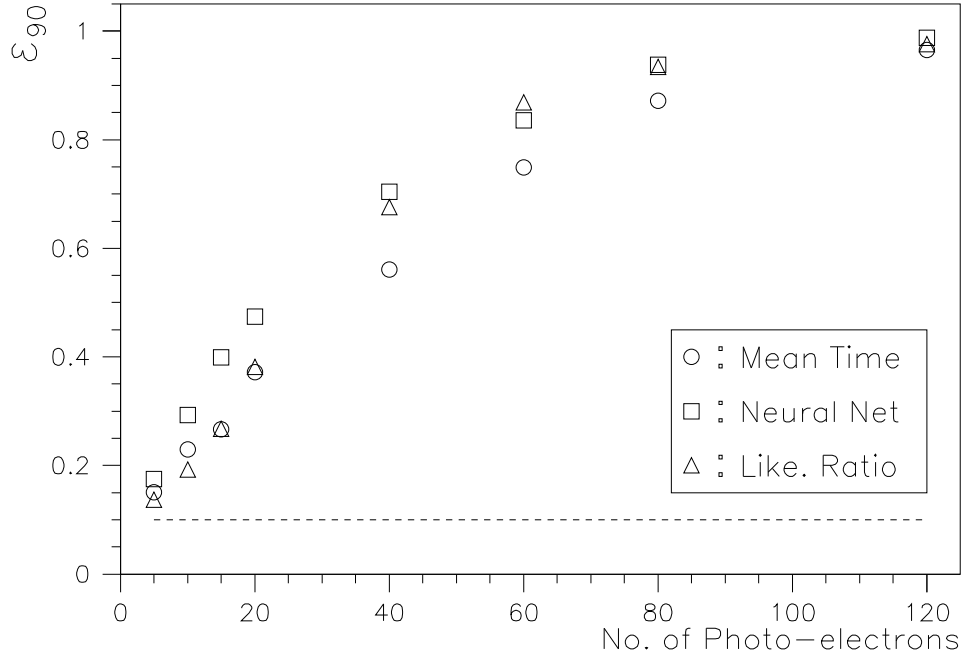


Figure 6: Typical separations of the (a) $\langle t \rangle$, (b) $F(X)$, and (c) LR parameters at $N_{pe} = 20$ between nuclear recoil (D_{nr} , in solid histograms) and γ (D_γ , in dotted histograms) events with the mean time, neural network and likelihood ratio methods, respectively.

(a)



(b)

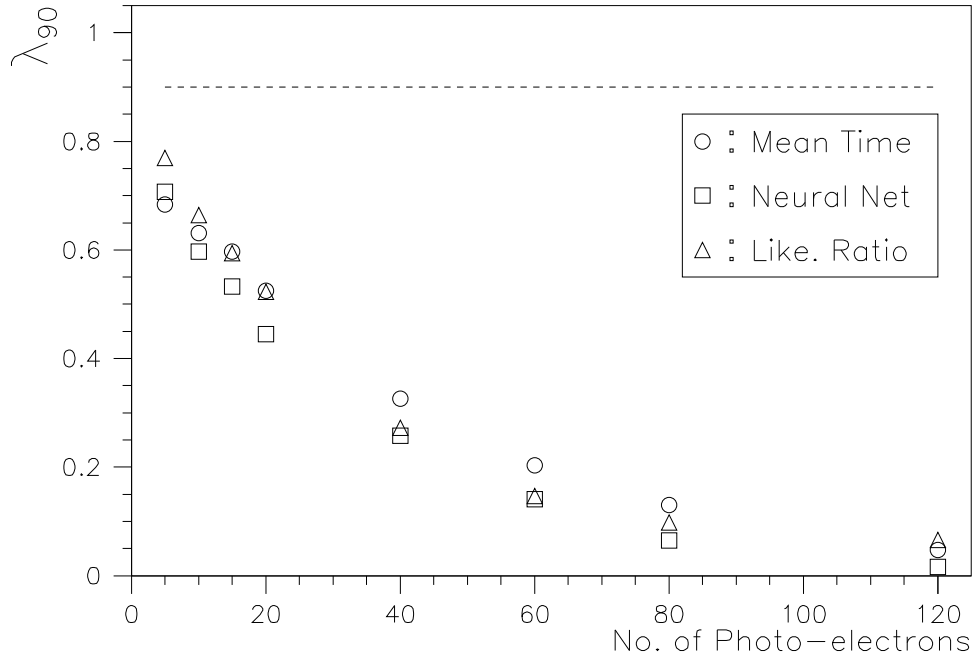


Figure 7: The variations of the figures of merit (a) ϵ_{90} and (b) λ_{90} with N_{pe} with the three different techniques applied to simulated nuclear recoil and γ data, respectively. Dotted lines indicate survival probabilities of γ and recoil events in (a) and (b), respectively. The statistical uncertainties are smaller than the data points.